Measurement 259 (2026) 119581

Contents lists available at ScienceDirect

Measurement

journal homepage: www.elsevier.com/locate/measurement

# Mid-IR photothermal lens sensing for trace water detection in organic solvents

Hongtu Cheng [a,b], Gustavo V.B. Lukasievicz [a,c,*], Alicja Dabrowska [a], Nelson G.C. Astrath [a,d], Georg Ramer [a,e], Bernhard Lendl [a,**]

[a] Institute of Chemical Technologies and Analytics, TU Wien, 1060 Vienna, Austria
[b] School of Electrical Engineering and Automation, Wuhan University, 430072 Wuhan, China
[c] Department of Physics, Universidade Tecnológica Federal do Paraná, Medianeira, PR 85722-332, Brazil
[d] Department of Physics, Universidade Estadual de Maringá, Maringá, PR 87020-900, Brazil
[e] Christian Doppler Laboratory for Advanced Mid-Infrared Laser Spectroscopy in (Bio-)process Analytics, TU Wien, 1060 Wien, Austria

ARTICLE INFO

*Keywords:*
Mid-infrared spectroscopy
Liquid sensing
EC-QCL pump source
Water detection

ABSTRACT

Photothermal lens (PTL) spectroscopy has achieved great success in the study of materials due to its high sensitivity and versatility. In this work, using an external cavity quantum cascade laser (EC-QCL) as the pump beam source, the PTL technique is used for the detection of water in ethanol and chloroform. The strong and broad optical absorption of water at 1645 $cm^{-1}$, attributed to the H-O-H bending mode, allows the detection of traces of water in solvents using an excitation laser with emission in the mid-infrared. Investigation of the PTL signal response in the frequency domain reveals an exponential decrease in signal amplitude with increasing modulation frequency. The method is validated with the coulometric Karl Fischer (KF) titration. The PTL signal amplitude exhibited a linear correlation with water concentration in the solvents. The limit of detection (LOD) for water in ethanol was 556 ppm, while the LOD for chloroform was 3.5 ppm. Higher sensitivity has been observed for water detection in chloroform due to lower background optical absorption from the solvent.

## 1. Introduction

Photothermal effects are employed in several high-sensitivity measurement techniques used for the characterization of liquid samples. The photothermal phenomenon is induced in the sample and surrounding media when radiated by light. The medium absorbs light energy, causing an increase in temperature that can result in increased infrared emission, changes in the refractive index, and expansion. In particular, the mode-mismatched photothermal lens (PTL) technique has also been demonstrated to be a powerful method for chemical analysis [1–4]. In this configuration, an excitation laser with a Gaussian radial profile ($TEM_{00}$) pumps the sample, inducing a time-dependent temperature and refractive index gradient in the sample. Consequently, an optical element resembling a lens-like optical element will be formed, i.e., the so-called thermal lens. The PTL effect is detected by a second laser with a Gaussian radial profile and low power, called probe beam. As the probe beam passes through the PTL, depending on the thermo-optical properties of the sample, it diverges/converges, resulting in a decrease/increase in the central light intensity. By measuring the light intensity change at the center of the probe beam, information about optical, thermal, and thermo-optical properties of the sample can be deduced. At present, there have been numerous studies showing that the photothermal lens technique has many application scenarios in liquids, including detection of acoustic wave [5,6], investigation of Soret effect [7–9] and photochemical reactions [9,10], determination of physical properties of liquids and mixtures [5–12], high-sensitive optical detection in flow injection analysis microchip devices [13–16] and detection in HPLC [17], study of the sample-surrounding heat coupling effect [18], and optimization of the PTL parameters for quantitative measurements [19–21].

Organic solvents are of fundamental importance in many industrial applications. Due to their application in multiple industrial operations, great efforts are made to develop methods for determining their trace impurity contents. In this context, water represents an impurity that negatively impacts solvent quality. Even at trace levels, water can disrupt chemical reactions, cause equipment damage, and affect the

* Corresponding author at: Department of Physics, Universidade Tecnológica Federal do Paraná, Medianeira, PR 85722-332, Brazil.
** Corresponding author at: Institute of Chemical Technologies and Analytics, TU Wien, 1060 Vienna, Austria.
*E-mail addresses:* gustavov@utfpr.edu.br (G.V.B. Lukasievicz), bernhard.lendl@tuwien.ac.at (B. Lendl).

https://doi.org/10.1016/j.measurement.2025.119581
Received 23 April 2025; Received in revised form 5 October 2025; Accepted 31 October 2025
Available online 3 November 2025

quality and yield of the products [22,23]. Therefore, as the water content of an organic solvent is an important indicator of its quality, the development of a rapid and sensitive method for the determination and control of trace water is necessary, and a range of advanced sensing systems have been developed to address this need [24–29]. Among various low humidity sensors, the Karl Fischer (KF) titration method is regarded as the gold standard for determining water traces in solvents. However, it requires expensive and toxic reagents, which will lead to sample consumption and waste generation [30–32]. Conventional analytical techniques also include chromatography [23] and NMR [33,34], which are time-consuming and cannot be used for online monitoring. Comparatively, optical sensors have the advantages of high sensitivity and long working life, providing an alternative to conventional analytical techniques and achieving real-time monitoring in the industries.

The mid-infrared spectrum of liquid water consists of three main molecular vibrations: the antisymmetric ($\nu_3$) and the symmetric ($\nu_1$) O–H stretching vibration (in the 3800 – 3000 $cm^{-1}$ region), and the H-O–H bending vibration ($\nu_2 \sim 1645$ $cm^{-1}$). In addition, in liquid water one can also observe the so-called libration modes ($\nu_L \sim 600$ $cm^{-1}$) due to hindered rotation of water molecules as well as a weak combination band at 2130 $cm^{-1}$ resulting from $\nu_L$ and $\nu_2$ [35–37]. Most mid-IR spectroscopic studies of water and aqueous solutions concern molecular interactions taking place within water molecules, solutes and surfaces. In this regard, the two stretching modes whose positions are strongly influenced by intermolecular forces, such as hydrogen bonding, have been used. Recently, it has been shown that also the position of the $\nu_2$ band can also serve as a good probe for structural investigations [37,38]. The use of tunable mid-infrared lasers addressing the $\nu_2$ band can thus make the detection system also sensitive to the chemical environment in which the water molecules are located.

In this paper, we developed a PTL liquid detection system employing an external cavity quantum cascade laser (EC-QCL) in the mid-infrared range as the pump source, and capable of covering the spectrum of water $\nu_2$~1645 $cm^{-1}$ in solvents. Two kinds of liquid, ethanol and chloroform, were selected as solvents. A series of experimental studies and analyses were carried out on a variety of samples, using the KF titration method as a reference. Compared to our previous work in which we used the same EC-QCL source but employed a photothermal Mach-Zehnder Interferometer for trace water detection [32], the experimental platform presented here is experimentally simpler as it requires only a single flow cell albeit providing comparable LODs for water in ethanol and in chloroform.

## 2. Experimental Description

The schematic diagram of dual-beam photothermal lens configuration is presented in Fig. 1. The excitation beam, also known as the pump beam, is focused on the liquid cell to induce a temperature gradient and change sample properties ('PTL effect region' in Fig. 1). This alteration causes the probe beam to diverge due to the negative thermo-optic coefficient of the sample, resulting in a decrease in light intensity at the detector. Modulating the pump beam at a specific frequency enables the detection of cyclic fluctuations in light intensity using a detector equipped with a small pinhole in front of it.

The experimental setup used in this work is shown in Fig. 2. The probe source was a linearly polarized helium–neon (HeNe) laser (Melles Griot, Rochester, NY, USA) with an emission wavelength of 632.8 nm and a power of 0.5 mW. A commercially available EC-QCL (DRS Daylight Solutions Inc., San Diego, CA, USA) was employed as the pump source, featuring tunability ranging from 1566 to 1720 $cm^{-1}$. The EC-QCL was set to a constant current of 650 mA and operated in CW mode (maximum power < 300 mW). The laser chip itself was temperature controlled by a thermoelectric cooler. An additional water cooler was used to dissipate the heat produced by the internal cooler to maintain the operating temperature of the laser head at 18 °C. The excitation laser was reflected by two gold mirrors, $M_{q1}$ and $M_{q2}$, and then modulated by a mechanical chopper (Thorlabs, MC2000B-EC) with a duty cycle of 50 %. Subsequently, the beam was reflected by a gold mirror $M_{q3}$ and then focused by a 100 mm focal length lens $L_2$ ($CaF_2$). After that, the beam was directed towards a custom-made ZnSe beam combiner (BC) with a maximum reflection at 633 nm and maximum transmission at 10.6 μm (Laser Components, Olching, Germany). The probe beam was reflected by the mirror $M_{p1}$ (silver), focused by a lens $L_1$ (N-BK7) with a focal length of 100 mm, and then reflected by the mirror $M_{p2}$ (silver) to reach the BC, where the two beams converged and followed a collinear configuration as they entered the liquid cell. The liquid transmission cell consisted of two 2-mm-thick $CaF_2$ windows, separated by an 85.8 μm PTFE spacer, which defined the optical pathlength or sample thickness. $M_{p3} \sim M_{p8}$ were six silver mirrors which were utilized to extend the optical path for the propagation of the probe beam, thereby ensuring that the photodetector was located in the far field. In front of the photodetector, a small pinhole with an inner diameter of 1 mm was placed. A photodiode (Thorlabs, DET10A) was used to detect the probe beam intensity. The signals were processed by a lock-in amplifier (LIA) (Zurich Instruments, MFLI) using the modulation frequency of the chopper as reference to obtain the amplitude of the PTL signal. An oscilloscope (Rigol, DS1104Z Plus) was used for recording the PTL time-domain signal. Table 1 presents the parameters of the experimental setup, in which the probe beam's cross section was analyzed by a dual scanning slit beam profiler (Thorlabs, BP209IR1/M), while the parameters of the pump beam were measured by a pyroelectric array laser beam profiler (Spiricon, Pyrocam IIIHR) operating in the mid-IR range.

Ethanol absolute, anhydrous with a purity of ≥ 99.8 % (max. 0.003 % $H_2O$) and chloroform stabilized (max. 0.005 % $H_2O$) were purchased from VWR Chemicals (Vienna, Austria). Initially, the solvents

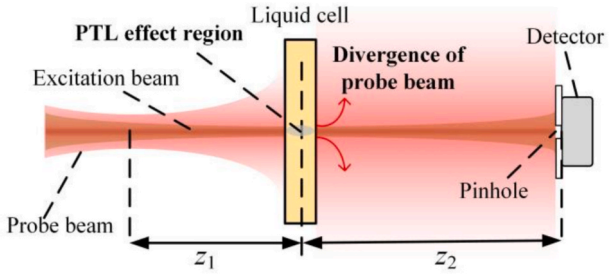


**Fig. 1.** Schematic diagram of dual-beam photothermal lens configuration. $z_1$ is the distance from the probe beam waist to the sample, $z_2$ is the distance from the sample to the detector.

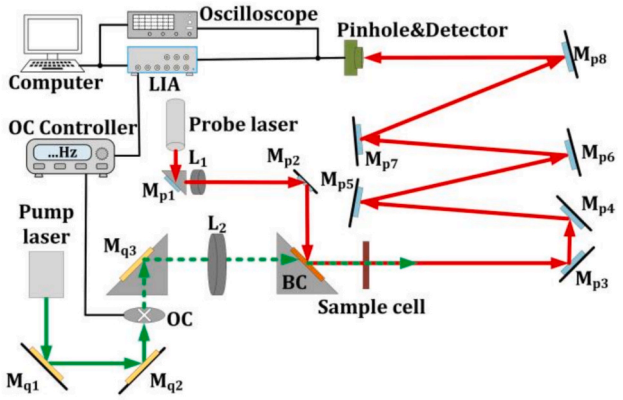


**Fig. 2.** Experimental setup for PTL-based liquid sensing. $M_{q1} \sim M_{q3}$ were used to reflect the pump beam; $M_{p1} \sim M_{p8}$ were used to reflect the probe beam; BC: beam combiner; OC: optical chopper; LIA: lock-in amplifier.

**Table 1**
Experimental parameters of the optical elements and structure.

| Parameter | Description | Value |
|---|---|---|
| $\lambda_p$ | Wavelength of probe beam | 632.8 nm |
| $\omega_{0p}$ | Radius of beam waist of probe beam | 82.3 μm |
| $\omega_{1p}$ | Beam radius of probe beam at sample cell | 625 μm |
| $z_1$ | Distance from the beam waist of probe beam to the liquid cell | 22 cm |
| $z_2$ | Distance from liquid cell to detector | 315 cm |
| $\omega_{0e}$ | Beam waist radius of the pump beam | ~450 μm |
| $\lambda_e$ | Emission wavenumber | 1566 $cm^{-1}$ to 1720 $cm^{-1}$ |
| $P_e$ | Power of pump laser at the sample | |
| | at 1602 $cm^{-1}$ (6.242 μm) | 39.0 mW |
| | at 1662 $cm^{-1}$ (6.017 μm) | 48.6 mW |

underwent a drying process. Aliquots of approximately 100 mL of ethanol and chloroform were mixed with molecular sieve pearls (3 Å for ethanol and 4 Å for chloroform) to establish a baseline solution for subsequent measurements. For ethanol samples, proper amounts of ultrapure water (resistivity: 18 MΩ • cm) were dissolved in dried ethanol to create solutions of different concentrations. For chloroform samples, an aliquot of chloroform was mixed with an equal volume of ultrapure water to prepare a saturated solution. The mixture was sonicated (30 min to 1 h) and was left overnight in a separatory funnel for phase separation, yielding chloroform saturated with water. Finally, mixtures of dried chloroform and saturated chloroform were mixed to obtain intermediate concentrations of water in chloroform. The prepared standards were first used to establish calibration curves using the PTL setup and were promptly analyzed afterward for their water content using the KF titrator (envirotech CA-21, Düsseldorf), which served as the reference method for determining water content in the prepared samples. We conducted three repetitions for each titration and calculated the mean value.

To obtain reference IR absorption spectra of water in each solvent, we employed a Tensor 37 FTIR spectrometer (Bruker corp., Ettlingen, Germany), equipped with a Globar and a liquid nitrogen-cooled MCT detector (D*=6.0 • $10^8$ cm $Hz^{1/2}$/W at 9.2 μm). The liquid transmission cell used for the measurements had an optical pathlength of 100 μm for ethanol and 300 μm for chloroform. A total of 256 scans were recorded per spectrum with a spectral resolution of 2 $cm^{-1}$. The instrument was continuously flushed with dry air prior- and throughout data acquisition. Spectra of water in the two solvents were measured against the respective pure (dried) solvent as background.

## 3. Results and Discussion

### 3.1. Water spectrum measured by FTIR

The recorded reference FTIR absorption spectra are depicted in Fig. 3. It is evident that the bending vibration of water ($\nu_2$) in ethanol and chloroform are located at approximately 1662 $cm^{-1}$ (6.017 μm) and 1602 $cm^{-1}$ (6.242 μm), respectively, which is in accordance with

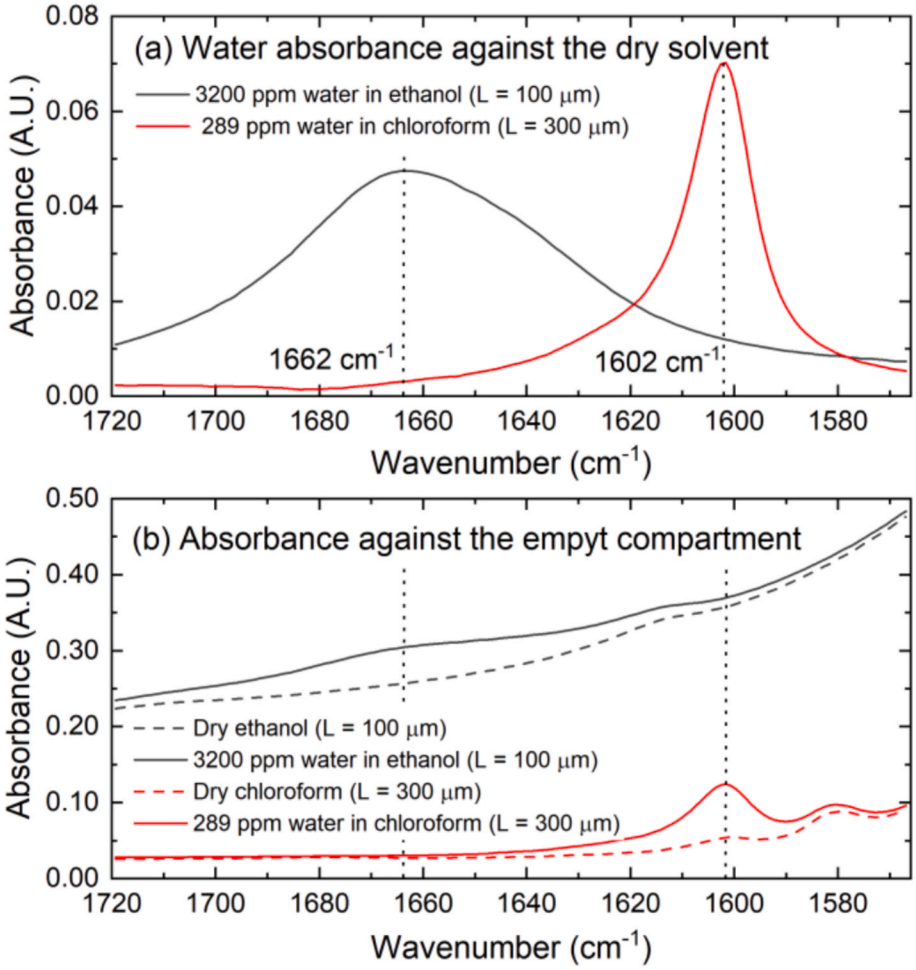


**Fig. 3.** (a) Water absorbance spectra measured using FTIR spectrometer, calculated relative to the corresponding dry solvent, for samples containing 3200 ppm water in ethanol and 289 ppm water in chloroform. (b) Absorbance spectra calculated relative to the background spectrum acquired from an empty FTIR sample compartment. Dashed lines represent the dry solvents; solid lines correspond to samples containing trace amounts of water.

findings in the literature [32,39,40]. Here we show the spectral region which is also accessible by the used EC-QCL source and thus of relevance for this work. The shift in band positions and band width of the bending vibration of water results from different intermolecular interactions in the protic solvent (ethanol) compared to the aprotic solvent (chloroform), particularly due to the absence of hydrogen bond interactions between water and chloroform. These identified peak positions served as reference points for quantification of the water content using the PTL setup.

Fig. 3(a) shows the water absorbance spectra obtained by subtracting the dry solvent spectrum from the FTIR measurements. In contrast, Fig. 3b presents spectra calculated with respect to the empty compartment of the FTIR, where the dashed lines correspond to the dry solvents and the solid lines to the samples containing trace amounts of water. The spectra in Fig. 3(a) therefore represent only the absorption of water in the solvents, whereas those in Fig. 3(b) reflect the combined absorption of both the solvent and water.

### 3.2. PTL frequency response characteristics

To find the optimal modulation frequency of the chopper, we explored the PTL frequency response characteristics. As an illustrative example, we show the results of water detection in chloroform. We set the laser's emission wavenumber to 1602 $cm^{-1}$ and changed the modulation frequency of the chopper to obtain both the PTL time-domain and frequency-domain signals. In Fig. 4(a), we present the PTL signals of a chloroform sample with a water concentration of 289 ppm at modulation frequencies of 20 Hz, 30 Hz and 100 Hz. The results show that the amplitude of the PTL signal decreases with the modulation frequency. To show more clearly the difference in the PTL amplitude for samples with different water content, the normalized PTL signal is calculated by dividing the value at each sample point by the maximum value measured during the time interval. In Fig. 4(b) we depict the normalized PTL signals for pure chloroform and 289 ppm water/chloroform at 20 Hz. It is apparent that water exerts an influence on the PTL amplitude signal. It can be observed that the signal intensity of 289 ppm of water in chloroform is higher than that of pure chloroform due to a higher optical absorption coefficient.

We also used a LIA to collect the PTL frequency domain signals. We set the time constant to 100 ms and plotted the obtained signals at different modulation frequencies in Fig. 5. In Fig. 5(a), the black dots represent the signal of pure chloroform, serving as the background signal, while the red dots represent the signal of 289 ppm of water in chloroform. The brown dots in Fig. 5(b) represent the relative signals, which were obtained by subtracting the background signal from the 289 ppm water/chloroform sample signal, i.e., the red dots subtracted from the black dots in Fig. 5(a).

It is evident that the PTL signal of the pure solvent, the sample with trace of water, and the relative signal decrease exponentially as the modulation frequency increases. We measured the signal-to-noise ratio (SNR) at modulation frequencies between 20 and 200 Hz to optimize the laser modulation frequency for quantifying water content. The SNR was calculated as the ratio of the photothermal signal amplitude to the noise level recorded with the lock-in amplifier in the pure solvent. Based on these results, 30 Hz was selected as the optimum chopper frequency, providing a higher SNR and photothermal lens (PTL) signal amplitude,

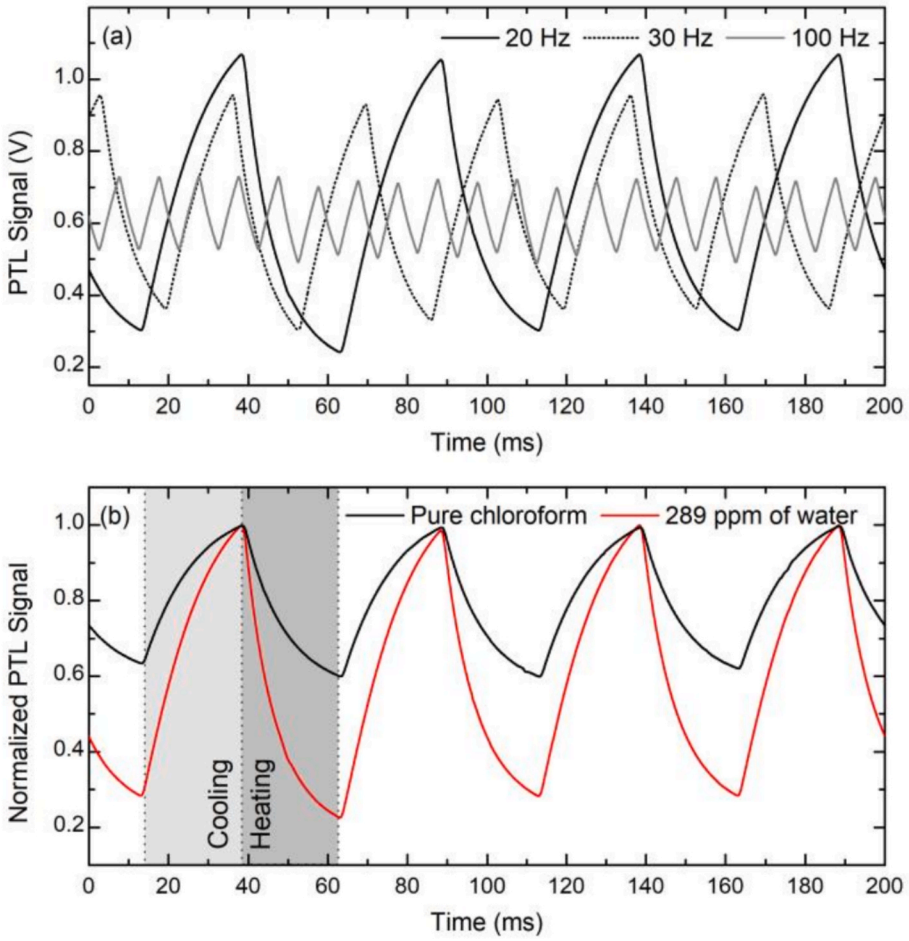


**Fig. 4.** PTL signals in time-domain, (a) PTL signals of chloroform (289 ppm of water) under the modulation frequency of 20 Hz, 30 Hz, and 100 Hz, (b) Normalized PTL signals of pure chloroform and water in chloroform under the modulation frequency of 20 Hz.

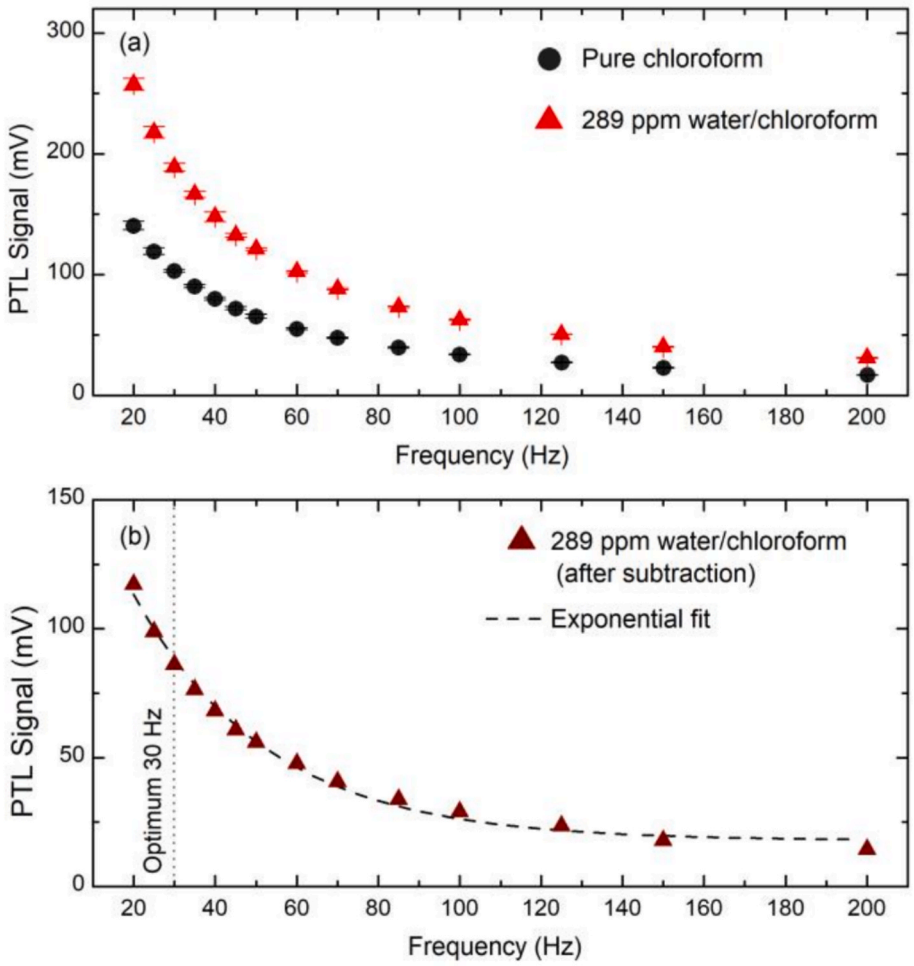


**Fig. 5.** Frequency response characteristics in the frequency domain, (a) PTL signals amplitude of pure chloroform and 289 ppm water/chloroform mixture, (b) signal amplitude after subtracting the pure chloroform signal from the signal of 289 ppm water/chloroform mixture.

while maintaining a relatively low modulation frequency. It should be emphasized that, considering the short laser exposure time (tens of milliseconds), the low water content in the organic solvent (< 0.4 wt%), and the limited liquid thickness (<100 μm), the contribution of the Soret effect can be neglected in this study.

### 3.3. Quantification of water content using the PTL setup

We measured samples with different water concentrations in chloroform and ethanol using the PTL setup. The results are shown in Fig. 6, in which the lower limit of detection (LOD) was calculated as $LOD = 3\sigma/Y_{slope}$, where $\sigma$ is the standard deviation, $Y_{slope}$ is the slope of the calibration line. The thermal lens signal amplitude depends on several experimental parameters, such as optical absorption, thermo-optical coefficient, thermal conductivity, liquid thickness (cell pathlength), as well as geometric parameters of the laser beams and laser excitation power. Therefore, the dynamic range of this method can vary considerably depending on the experimental setup used. For higher water content, nonlinearity may occur due to an increase in the optical absorption coefficient, leading to photothermal saturation. This term is used to describe the effect in which the photothermal signal fails to vary linearly with absorption coefficient at high values [1,41]. To prevent signal saturation, we incorporated a 10 % transmittance attenuator between $M_{q1}$ and $M_{q2}$ in the experimental setup shown in Fig. 2, reducing the excitation beam's power at the sample position to 4.9 mW at 1662 $cm^{-1}$. This allows us to use the same liquid cell, with equal optical pathlength, to measure both water in ethanol and water in chloroform. Additionally, it can be observed that the calibration line of water in ethanol has an offset of approximately 6.2 mV, while the offset for water in chloroform is approximately 64.1 mV, which can be attributed to the absorption by the solvent itself. Even for the pure solvents, the PTL signal can be significant, as it is possible to observe in Figs. 4-6.

KF titration is the mainstay method for determining water content in routinely used organic solvents. It is applicable to a wide range of matrices, including organic solvents, oils, pharmaceutical products, petrochemicals, and jet fuel. Using typical sample portions of 5–10 g, KF titration achieves LODs in the low ppm range (e.g., ~1 ppm for a 10 g sample in coulometric mode, or ~ 12.5 ppm for a 5 g sample in volumetric mode) [28,29]. For these reasons, the KF titration method was selected as the calibration reference in this work (Fig. 6). For comparison, gas chromatography–mass spectrometry with selected ion monitoring (GC–MS–SIM) achieves similar LODs in the ppm range (e.g., 5 ppm) [23], whereas NMR spectroscopy yields LODs that depend on the solvent and experimental conditions, ranging from a few ppm to several hundred ppm [33,34]. Also, NIR spectroscopy has been proposed for direct, reagent free water quantification in organic solvents [42]. Recently a miniaturized NIR spectrometer, operating in the short-wave part of the NIR spectrum (740–1070 nm), has been adapted for determining water in solvents showing precision of ~ 0.01 wt% in the 0–0.25 wt% concentration range for water in methyl ethyl ketone (MEK) [43]. A comprehensive overview on optical techniques for determination of water in solvents comprising spectrophotometric and spectrofluorimetric methods but requiring reagents or dedicated sensor

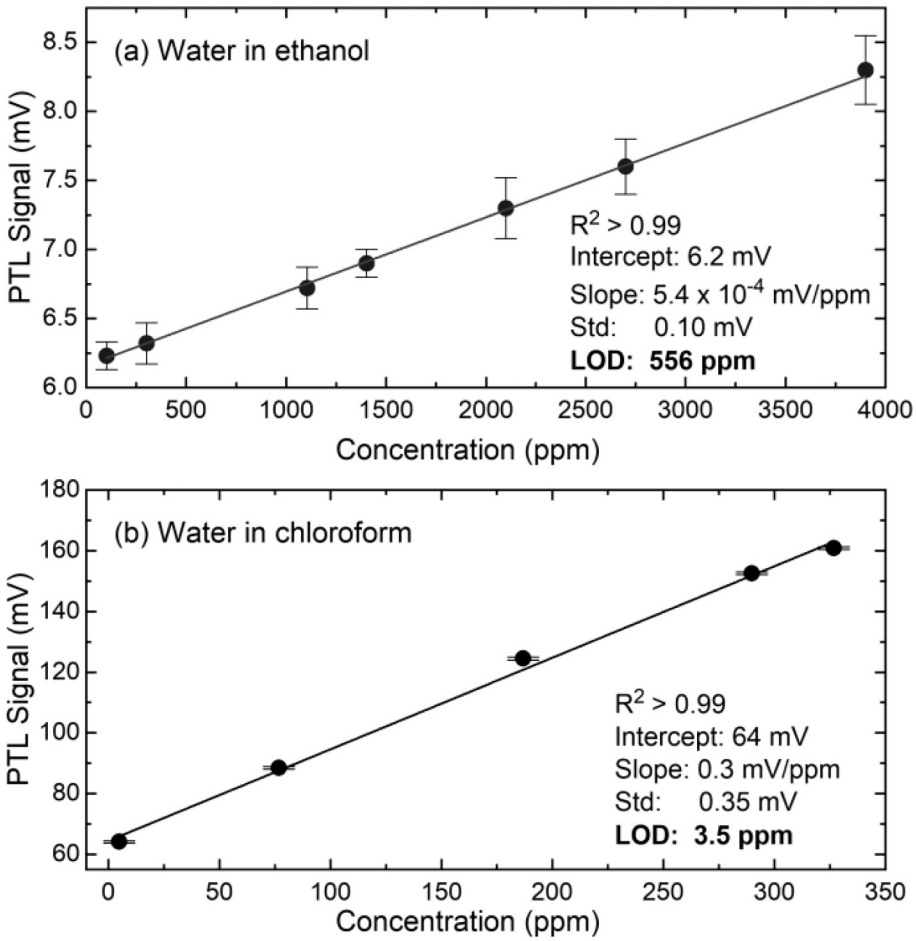


**Fig. 6.** Calibration curves of PTL signal versus water concentration (average of 20 repetitions) for (a) ethanol and (b) chloroform. The data are shown together with the corresponding linear regression fits.

materials can be found in [44].

The PTL signal demonstrates a linear relationship with water concentration. The LOD for water in ethanol and chloroform are 556 ppm and 3.5 ppm, respectively. The LOD obtained by the PTL technique, with a simpler optical layout, shows similar performance to the photothermal Mach-Zehnder interferometry (PT-MZI), which obtained LOD of 400 ppm and 7.4 ppm for water in ethanol and chloroform, respectively [32].

The PT-MZI technique requires interferometric alignment and is highly sensitive to environmental perturbations such as vibrations, temperature fluctuations, and air currents. In contrast, the PTL configuration eliminates the need for interferometric detection arms and active stabilization, thereby reducing instrumentation complexity and signal processing demands. These features can lower maintenance requirements and improve accessibility for routine use. Additionally, the PTL approach can be easily adapted to different solvents or analytes without the need for significant re-optimization of the optical setup. This versatility makes it suitable for a broader range of analytical applications.

The lower LOD for water detection in chloroform, as opposed to water detection in ethanol, can be explained by several factors. Apart from using a reduced laser excitation power for water determination in ethanol, chloroform exhibits higher photothermal enhancement factor $E=(dn/dT)/k$, where $dn/dT$ is thermo-optical coefficient and $k$ is the thermal conductivity. Also, chloroform shows a significantly lower background optical absorption compared to ethanol (see Fig. 3(b)). Consequently, more of the laser power can be absorbed by the analyte and not by the solvent. Furthermore, assuming the same amount of heat released into the solvent, a stronger thermal lens is developed in chloroform as opposed to ethanol due to its higher thermo-optical coefficient and lower thermal conductivity.

## 4. Conclusions

In this study, we present a PTL liquid sensing setup which uses an EC-QCL as a mid-IR pump source and a HeNe laser as probe beam in a colinear sensing arrangement. We measured the reference spectra of water in ethanol and chloroform using an FTIR spectrometer to select the optimum measurement wavelengths for achieving highest sensitivity when using the mid-IR laser for sample excitation. Maximum water absorption of the water bending vibration was observed at 1662 $cm^{-1}$ for chloroform and at 1602 $cm^{-1}$ for ethanol, respectively. Subsequently, we investigated the time and frequency domain PTL signals under various modulation frequencies. We found that the amplitude of PTL signals displayed an exponential decrease with increasing modulation frequency. We prepared samples with different water content for ethanol and chloroform and observed a linear relationship between PTL signals and water concentration. The LOD for water was determined to be 556 ppm in ethanol and 3.5 ppm in chloroform. Our comparative analysis of detection limits indicates that PTL achieves performance comparable to that of PT-MZI, while providing clear advantages in simplicity, cost, and operational flexibility. The PTL method requires only a single flow cell and eliminates the need for interferometric detection arms or active stabilization systems, thereby simplifying both instrumentation and data processing. Furthermore, the PTL approach can be readily adapted to different solvents or analytes without

extensive re-optimization of the optical setup, enhancing its versatility for a wide range of analytical applications.

## CRediT authorship contribution statement

**Hongtu Cheng:** Writing – original draft, Visualization, Methodology, Investigation, Formal analysis, Data curation. **Gustavo V.B. Lukasievicz:** Writing – original draft, Visualization, Methodology, Investigation, Formal analysis, Supervision, Writing – review & editing. **Alicja Dabrowska:** Visualization, Methodology, Investigation, Formal analysis. **Nelson G.C. Astrath:** Formal analysis, Investigation, Methodology. **Georg Ramer:** Methodology, Investigation, Formal analysis. **Bernhard Lendl:** Writing – review & editing, Supervision, Funding acquisition, Conceptualization, Resources.

## Declaration of competing interest

The authors declare that they have no known competing financial interests or personal relationships that could have appeared to influence the work reported in this paper.

## Acknowledgements

This study has received co-funding from the European Union's Horizon 2020 research and innovation programme under grant agreement no. 101057844 (Enviromed). Furthermore, the financial support by the Austrian Federal Ministry of Labour and Economy, the National Foundation for Research, Technology and Development, and the Christian Doppler Research Association is gratefully acknowledged. H. Cheng acknowledges support from the China Scholarship Council (202206270137). G. V. B. Lukasievicz and N. G. C. Astrath acknowledge support from CNPq (grant agreement No. 307415/2022-8, 305333/2023-2, 408454/2024-5) and the National Institute for Research and Innovation in Photothermal Imaging (INPIIF).

## Data availability

Data will be made available on request.

## References

[1] S.E. Bialkowski, N.G.C. Astrath, M.A. Proskurnin, Photothermal Spectroscopy Methods, second ed., John Wiley & Sons, 2019.
[2] M. Franko, C.D. Tran, Analytical thermal lens instrumentation, Rev. Sci. Instrum. 67 (1996) 1–18, https://doi.org/10.1063/1.1147512.
[3] M. Franko, L. Goljat, M. Liu, H. Budasheva, M.Ž. Furlan, D. Korte, Recent Progress and applications of thermal Lens Spectrometry and Photothermal Beam Deflection Techniques in Environmental Sensing, Sensors 23 (2023) 472, https://doi.org/10.3390/s23010472.
[4] M.J. Navas, A.M. Jiménez, Thermal Lens Spectrometry as Analytical Tool, Crit. Rev. Anal. Chem. 33 (2003) 77–88, https://doi.org/10.1080/713609156.
[5] E.V. Bergmann, G.V.B. Lukasievicz, B. Lendl, A.R. Sampaio, V.S. Zanuto, M. L. Baesso, L.C. Malacarne, N.G.C. Astrath, Optoacoustic detection of nanosecond time scale photoinduced lensing effects in liquids, J. Appl. Phys. 134 (2023) 165103, https://doi.org/10.1063/5.0172822.
[6] O.A. Capeloto, V.S. Zanuto, V.G. Camargo, G.A.S. Flizikowski, F.A.P. Morais, G.V. B. Lukasievicz, L.S. Herculano, M.P. Belançon, N.G.C. Astrath, L.C. Malacarne, Induction and detection of pressure waves by pulsed thermal lens technique in water–ethanol mixtures, Appl. Opt. 60 (2021) 4029–4033, https://doi.org/10.1364/AO.420275.
[7] N. Arnaud, J. Georges, Investigation of the thermal lens effect in water-ethanol mixtures: composition dependence of the refractive index gradient, the enhancement factor and the Soret effect, Spectrochim. Acta, Part A 57 (2001) 1295–1301, https://doi.org/10.1016/S1386-1425(00)00465-0.
[8] H. Cabrera, E. Sira, K. Rahn, M. García-Sucre, A thermal lens model including the Soret effect, Appl. Phys. Lett. 94 (2009) 051103, https://doi.org/10.1063/1.3078287.
[9] L.C. Malacarne, N.G.C. Astrath, A.N. Medina, L.S. Herculano, M.L. Baesso, P.R. B. Pedreira, J. Shen, Q. Wen, K.H. Michaelian, C. Fairbridge, Soret effect and photochemical reaction in liquids with laser-induced local heating, Opt. Express 19 (2011) 4047–4058, https://doi.org/10.1364/OE.19.004047.
[10] L.S. Herculano, L.C. Malacarne, V.S. Zanuto, G.V.B. Lukasievicz, O.A. Capeloto, N. G.C. Astrath, Investigation of the Photobleaching Process of Eosin Y in Aqueous solution by thermal Lens Spectroscopy, J. Phys. Chem. B 117 (2013) 1932–1937, https://doi.org/10.1021/jp3119296.
[11] A. Mërtiri, T. Jeys, V. Liberman, M.K. Hong, J. Mertz, H. Altug, S. Erramilli, Mid-infrared photothermal heterodyne spectroscopy in a liquid crystal using a quantum cascade laser, Appl. Phys. Lett. 101 (2012) 044101, https://doi.org/10.1063/1.4737942.
[12] H. Cabrera, J. Akbar, D. Korte, I. Ashraf, E.E. Ramírez-Miquet, E. Marín, J. Niemela, Absorption Spectra of Ethanol and Water using a Photothermal Lens Spectrophotometer, Appl. Spectrosc. 72 (2018) 1069–1073, https://doi.org/10.1177/0003702818759073.
[13] M. Franko, Thermal Lens Spectrometric Detection in Flow Injection Analysis and Separation Techniques, Appl. Spectrosc. Rev. 43 (2008) 358–388, https://doi.org/10.1080/05704920802108032.
[14] K. Mawatari, T. Ohashi, T. Ebata, M. Tokeshi, T. Kitamori, Thermal lens detection device, Lab Chip 11 (2011) 2990–2993, https://doi.org/10.1039/C1LC20175A.
[15] T. Kitamori, Thermal Lens Microscope and Microchip Chemistry, Bull. Chem. Soc. Jpn 92 (2019) 469–473, https://doi.org/10.1246/bcsj.20180276.
[16] M. Liu, M. Franko, Progress in thermal Lens Spectrometry and its applications in Microscale Analytical Devices, Crit. Rev. Anal. Chem. 44 (2014) 328–353, https://doi.org/10.1080/10408347.2013.869171.
[17] M.A. Proskurnin, A.Y. Luk'yanov, S.N. Bendrysheva, A.A. Bendryshev, A. V. Pirogov, O.A. Shpigun, Optical photothermal detection in HPLC, Anal Bioanal Chem 375 (2003) 1204–1211, https://doi.org/10.1007/s00216-002-1720-1.
[18] G.V.B. Lukasievicz, L.S. Herculano, E. Sehn, M.P. Belançon, S.E. Bialkowski, O. A. Capeloto, N.G.C. Astrath, L.C. Malacarne, An Experimental Investigation of Sample-Fluid Heat Coupling effect in thermal Lens Technique, Appl. Spectrosc. 74 (2020) 1274–1279, https://doi.org/10.1177/0003702820937364.
[19] R. Silva, M.A.C. de Araújo, P. Jali, S.G.C. Moreira, P. Alcantara, P.C. de Oliveira, Thermal lens spectrometry: Optimizing amplitude and shortening the transient time, AIP Adv. 1 (2011) 022154, https://doi.org/10.1063/1.3609966.
[20] R. Hannachi, Photothermal lens spectrometry: Experimental optimization and direct quantification of permanganate in water, Sens. Actuators B Chem. 333 (2021) 129542, https://doi.org/10.1016/j.snb.2021.129542.
[21] B. Abbasgholi-NA, A. Rahman, F. D'Amico, H. Cabrera, Led-based thermal lens spectrometry with a double-pass probe beam optimized configuration: a complete feasibility study, Measurement 252 (2025) 117392, https://doi.org/10.1016/j.measurement.2025.117392.
[22] G.P. Moore, A.B. Dichiara, Classification and quantification of water and organic solvent mixtures using paper-based sensors coupled with machine learning, Sens. Actuators B 437 (2025) 137735, https://doi.org/10.1016/j.snb.2025.137735.
[23] B.Q. Xu, C.Q. Rao, S.F. Cui, J. Wang, J.L. Wang, L.P. Liu, Determination of trace water contents of organic solvents by gas chromatography-mass spectrometry-selected ion monitoring, J. Chromatogr. A 1570 (2018) 109–115, https://doi.org/10.1016/j.chroma.2018.07.068.
[24] Y. Li, C. Deng, M. Yang, A novel surface acoustic wave-impedance humidity sensor based on the composite of polyaniline and poly (vinyl alcohol) with a capability of detecting low humidity, Sens. Actuators B Chem. 165 (2012) 7–12, https://doi.org/10.1016/j.snb.2011.12.037.
[25] T. Islam, L. Kumar, S.A. Khan, A novel sol-gel thin film porous alumina based capacitive sensor for measuring trace moisture in the range of 2.5-25 ppm, Sens. Actuators B Chem. 173 (2012) 377–384, https://doi.org/10.1016/j.snb.2012.07.014.
[26] Z. Ma, T. Fei, T. Zhang, An overview: Sensors for low humidity detection, Sens. Actuators B Chem. 376 (2023) 133039, https://doi.org/10.1016/j.snb.2022.133039.
[27] M.S. Ghoraishi, J.E. Hawk, M.F. Arindam Phani, T.T. Khan, Clustering mechanism of ethanol-water mixtures investigated with photothermal microfluidic cantilever deflection spectroscopy, Sci. Rep. 6 (2016) 23966, https://doi.org/10.1038/srep23966.
[28] F. Pilat, B. Schwarz, B. Baumgartner, D. Ristanić, H. Detz, A.M. Andrews, B. Lendl, G. Strasser, B. Hinkov, Beyond Karl Fischer titration: a monolithic quantum cascade sensor for monitoring residual water concentration in solventes, Lab Chip 23 (2023) 1816–1824, https://doi.org/10.1039/D2LC00724J.
[29] P. Kumar, A. Ghosh, D.A. Jose, Chemical Sensors for Water Detection in Organic Solvents and their applications, ChemistrySelect 6 (2021) 820–842, https://doi.org/10.1002/slct.202003920.
[30] E. Scholz, K. Fischer, Titration: Determination of Water, Springer Science & Business Media, 2012.
[31] P. Rivera-Quintero, G.S. Patience, N.A. Patience, D.C. Boffito, X. Banquy, D. Schieppati, Experimental methods in chemical engineering: Karl Fischer titration, Can. J. Chem. Eng. 102 (2024) 2980–2997, https://doi.org/10.1002/cjce.25295.
[32] G. Ricchiuti, A. Dabrowska, D. Pinto, G. Ramer, B. Lendl, Dual-Beam Photothermal Spectroscopy Employing a Mach–Zehnder Interferometer and an External Cavity Quantum Cascade Laser for Detection of Water Traces in Organic Solvents, Anal. Chem. 94 (2022) 16353–16360, https://doi.org/10.1021/acs.analchem.2c03303.
[33] E. Kang, H.R. Park, J. Yoon, H.Y. Yu, S.K. Chang, B. Kim, K. Choi, S. Ahn, A simple method to determine the water content in organic solvents using the $^{1}$H NMR chemical shifts differences between water and solvent, Microchem. J. 138 (2018) 395–400, https://doi.org/10.1016/j.microc.2018.01.034.
[34] X. Creary, No-Deuterium Proton (No-D) NMR as a Convenient Method for Analysis of Organic Solvents, J. Org. Chem. 88 (16) (2023) 11545–11551, https://doi.org/10.1021/acs.joc.3c00807.
[35] E. Zoidis, J. Yarwood, T. Tassaing, Y. Danten, M. Besnard, Vibrational spectroscopic studies on the state of aggregation of water in carbon tetrachloride,

in dioxane and in the mixed solvents, J. Mol. Liq. 64 (1995) 197–210, https://doi.org/10.1016/0167-7322(95)00816-S.
[36] P.K. Verma, A. Kundu, M.S. Puretz, C. Dhoonmoon, O.S. Chegwidden, C. H. Londergan, M. Cho, The Bend+Libration Combination Band is an Intrinsic, Collective, and strongly Solute-Dependent Reporter on the Hydrogen Bonding Network of Liquid Water, J. Phys. Chem. B 122 (2018) 2587–2599, https://doi.org/10.1021/acs.jpcb.7b09641.
[37] T. Seki, K.Y. Chiang, C.C. Yu, X. Yu, M. Okuno, J. Hunger, Y. Nagata, M. Bonn, The Bending Mode of Water: a Powerful Probe for Hydrogen Bond Structure of Aqueous Systems, J. Phys. Chem. Lett. 11 (2020) 8459–8469, https://doi.org/10.1021/acs.jpclett.0c01259.
[38] T. Seki, S. Sun, K. Zhong, C.C. Yu, K. Machel, L.B. Dreier, E.H.G. Backus, M. Bonn, Y. Nagata, Unveiling Heterogeneity of Interfacial Water through the Water Bending Mode, J. Phys. Chem. Lett. 10 (2019) 6936–6941, https://doi.org/10.1021/acs.jpclett.9b02748.
[39] X. Yu, T. Seki, C.C. Yu, K. Zhong, S. Sun, M. Okuno, E.H.G. Backus, J. Hunger, M. Bonn, Y. Nagata, Interfacial Water Structure of Binary Liquid Mixtures Reflects Nonideal Behavior, J. Phys. Chem. B 125 (2021) 10639–10646, https://doi.org/10.1021/acs.jpcb.1c06001.
[40] D. Zhou, Q. Wei, H. Bian, J. Zheng, Direct Vibrational Energy transfer in Monomeric Water Probed with Ultrafast two Dimensional Infrared Spectroscopy, Chin. J. Chem. Phys. 30 (2017) 619–625, https://doi.org/10.1063/1674-0068/30/cjcp1710189.
[41] L. Bozec, A. Hammiche, H.M. Pollock, M. Conroy, J.M. Chalmers, N.J. Everall, L. Turin, Localized photothermal infrared spectroscopy using a proximal probe, J. Appl. Phys. 90 (2001) 5159–5165, https://doi.org/10.1063/1.1403671.
[42] S. Garrigues, M. Gallignani, M. de la Guardi, Flow-injection determination of water in organic solvents by near-infrared spectrometry, Anal. Chim. Acta 281 (1993) 259–264, https://doi.org/10.1016/0003-2670(93)85180-R.
[43] G.H. van Kollenburg, H.J. van Manen, N. Admiraal, J. Gerretzen, J.J. Jansen, Low-cost handheld NIR spectroscopy for identification of organic solvents and low-level quantification of water contamination, Talanta 223 (2021) 121865, https://doi.org/10.1016/j.talanta.2020.121865.
[44] A. Jouyban, E. Rahimpour, Optical sensors for determination of water in the organic solvents: a review, J. Iran. Chem. Soc. 19 (2022) 1–22, https://doi.org/10.1007/s13738-021-02290-0.